Proceedings World Geothermal Congress 2010
Bali, Indonesia, 25-29 April 2010

Modelling of Injection into Vapour-Dominated Geothermal Systems

Eylem Kaya and Michael O'Sullivan

Department of Engineering Science, University of Auckland, Private Bag 92019, Auckland, New Zealand

e.kaya@auckland.ac.nz and m.osullivan@auckland.ac.nz

Keywords: injection, reservoir modelling, vapor dominated reservoirs, fractured reservoirs.

ABSTRACT

A numerical model of a generic vapour-dominated geothermal reservoir is used to test various injection strategies. The model is based loosely on the Darajat system but the results should be relevant for other similar reservoirs such as Larderello, Kamojang and The Geysers. Model parameters such as vertical permeability, porosity and relative permeability are investigated. Different injection rates and start-times for injection are tried. Various aspects of model design such as grid refinement, use of an embedded radial grid near the wells, dual porosity and nine-point differencing are investigated.

1. INTRODUCTION

Vapour-dominated systems are characterised by a low immobile water fraction so that production wells discharge dry steam. Within the reservoir zone there are high temperatures and comparatively low boiling-point pressures.

Thus by their very nature, vapour-dominated two-phase systems have good permeability in the reservoir zone and very low permeability surrounding the reservoir. If this were not the case, cold water would flow into the low-pressure vapour-dominated reservoir from the surrounding cool rock. During production from this type of system, as reservoir pressures decrease, the immobile water boils to form steam which then flows towards the production wells. The water in a vapour-dominated reservoir is not replenished by natural recharge and, after some years of production, parts of the reservoir may run out of immobile water and become superheated (i.e. the temperature of the steam is above the boiling point).

In this paper a study of injection in vapour-dominated system is discussed. The Darajat geothermal field is chosen as the basis for the study for two reasons: first it is a typical vapour dominated geothermal system (Alamsyah et al. (2005), Hadi et al. (2005)) and secondly an existing computer model of Darajat was available at the University of Auckland.

Injection into vapor dominated reservoirs involves complex fluid flow and heat transfer processes including boiling and condensation, vapor-liquid counter-flow and mixing of waters with different temperatures. The TOUGH2 geothermal reservoir simulator (Pruess et al. (1999)) can model these physical processes including the highly non-linear phase transitions from vapour to two-phase and then to all-liquid conditions, together with the associated strongly coupling of fluid flow and heat transfer effects. However, this capability for simulating the basic processes does not necessarily guarantee accurate predictions for practical injection problems that involve multidimensional flow effects on a broad range of space and time scales (Pruess (1991)). Past modeling studies of vapour-dominated reservoir (Schroeder et. al (1982), Pruess (1994), Pruess (1995), Pruess (1996), Fitzgerald et al (1994), etc.) show that different models of a vapour-dominated reservoir may lead to very different predictions. The aim of the present study is to carry out sensitivity studies on a simple 2D model of a vapour-dominated geothermal reservoir in order to derive a good model which can produce an accurate prediction of injection effects.

2. MODEL DESCRIPTION

A 2D model was set up based on a typical vertical slice through the 3D model of Darajat. The model consists of a vertical slice 10km long, 250 m thick, 4350-4890 m deep and it consists of 17 layers. The rock in the outer zone has a very low permeability (0.04-0.16 md) to prevent cool water flooding the vapour-dominated zone. Similarly a low permeability cap-rock was assigned to the top of the reservoir.

The atmospheric conditions maintained at the ground surface are 1bar pressure and 15°C temperature. As shown by the modelling studies of O'Sullivan (1990) and McGuniness et al. (1993) it is not possible to produce a stable steady-state vapour-dominated system by applying constant mass and energy flows at the base of the model. By considering the stability of a 1-D heat pipe (counter-flow of liquid and steam driven by gravity in a uniform porous medium) McGuinness et al. (1993) showed that a vapour-dominated reservoir must have saturation control at depth. Therefore in the 2D model constant pressure and saturation boundary conditions (94.6 bar pressure and 0.25 vapour saturation) are applied at the base of the reservoir blocks. At the base of the model, outside the reservoir zone, a 0.06 W/m^2 heat input is applied as the base boundary condition.

The flow from the hot springs is represented by wells on deliverability. For the deliverability option wells produce against a prescribed flowing bottom-hole pressure, p_{wb}, with a productivity index PI (Pruess et al. (1999)). The mass production rate of phase β from a grid block with phase pressure $p_\beta > p_{wb}$ is given by;

$$q_\beta = \frac{k_{r\beta}}{\nu_\beta} PI(p_\beta - p_{wb}) \qquad (1)$$

Here q is mass flow, k_r is relative permeability, ν is kinematic viscosity, PI is productivity index, p is fluid pressure and p_{wb} is the wellbore pressure.

For all production and spring wells the DELG option (autough2 notes, (2002)) was used which allows a discharge proportional to the pressure above some cut-off value. Combining the flow of each phase given by (1) the total flow from the spring wells has the form

$$q_m = PI \frac{1}{\nu_f}(p - p_{cut-off}) \quad (2)$$

$$\frac{1}{\nu_f} = \frac{k_{rl}}{\nu_l} + \frac{k_{rv}}{\nu_v} \quad (3)$$

Where q_m is the mass flow, ν_f, ν_l and ν_v are the kinematic viscosities of the fluid, liquid and vapour, respectively, p is the reservoir pressure, $p_{cut-off}$ is the trigger pressure at which the well stops flowing, k_{rl} and k_{rv} are the relative permeabilities for the liquid and vapor phases, respectively. The parameters PI and $p_{cut-off}$ are adjusted to give mass flows from the hot springs in the model that matches the measured values.

2.1 Natural State

The aim of the first stage of modelling was to set up a 2D model that produced similar natural state conditions to those for the 3D Darajat model.

I. Model 1a: A North West - South East vertical slice through the 3D Darajat model was used to set up the 2D model. The vertical grid structure, permeability distribution, heat inputs, deliverability parameters for the spring blocks and boundary conditions from the 3D Darajat model were applied to this 2D model. Three spring blocks were used closest to the spring locations in the 3D model. Table 1 and Table 2 summarize the rock parameters, boundary conditions, deliverability conditions and relative permeability functions used in Model 1a.

Table 1: Rock parameters for Model 1a.

	Rock density kg/m^3	Porosity	Horizontal permeability, 10^{-15} m^2	Vertical permeability, 10^{-15} m^2
topk	2500	0.1	100	1.5
capk	2500	0.01	0.08	0.04
andd	2650	0.06	25	25
ande	2650	0.06	36	36
brcch	2500	0.09	12.5	12.5
brccm	2500	0.09	2.2	2.2
side1	2500	0.01	0.16	0.08
side2	2500	0.01	0.08	0.04
base1	2500	0.01	3	6
base2	2500	0.01	0.72	0.72

Table 2: Other parameters for Model 1a.

Rock properties	
Heat conductivity : 2.50W/m K	Specific heat : 1000 J/kg
Base boundary conditions for outer zone blocks	
Heat input: 0.06 W/m^2	No mass input
Base boundary conditions for the reservoir blocks	
Pressure: 126.0 bar	Vapour saturation: 0.25
Spring well parameters	
Productivity index : 1.09E-9 m^3	Cut-off pressure: 28 bar
Relative permeability (Linear curves)	
S_{lr} : 0.75 S_{vr}: 0.0 S_{pr}: 0.25	

II. Model 1b: Model 1a produced somewhat different results for pressure, temperature and vapour saturation to those from the 3D Darajat model. To achieve a better match with a simpler permeability structure the following modifications were applied to the springs and the base boundary conditions.

(a) Springs

The escape of steam from hot springs is represented by three wells on deliverability located under the caprock (black squares in Figure 1), while there are fifteen wells representing hot springs in the 3D model. To obtain similar pressure, temperature and vapour saturation profiles to the 3D model, the deliverability parameters of the spring wells were adjusted. The cut-off pressure was decreased from 28 bar to 20 bar while the PI was left unchanged.

(b) Permeability structure

The permeability structure of the original 3D model was simplified to include fewer rock types. The simplified structure is shown in Figure 1.

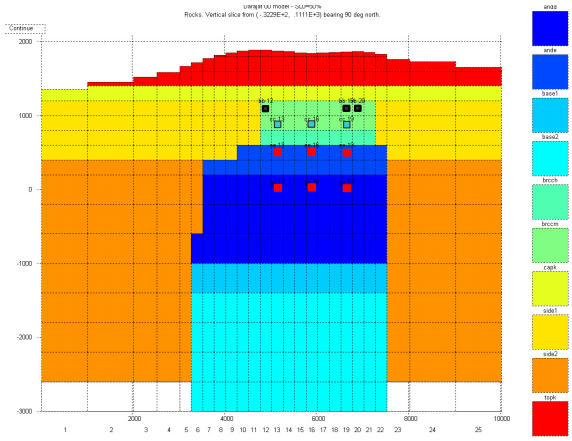

Figure 1: Permeability distribution for Model 1b.

(c) Base conditions

Considerable numerical experimentation was carried out to determine the effects of varying the base reservoir boundary conditions. It was found that increasing the base pressure increases the reservoir pressure up to a maximum value, but then a further increase in the deep boundary pressure resulted in a decreased reservoir pressure (see Figure 2).

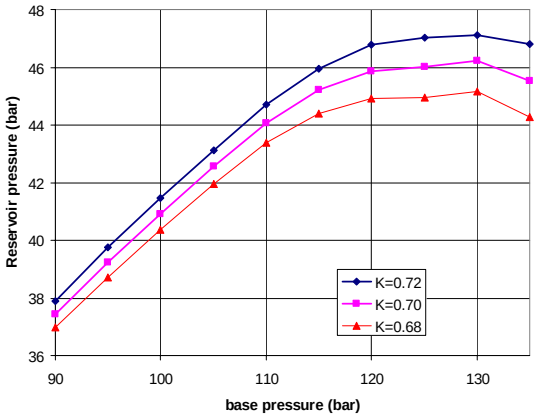

Figure 2: Effect of the base boundary pressure on the reservoir pressure for different basement permeabilities.

It was difficult to achieve steady state conditions for a base pressure greater than 135 bar and also it was found that the wet zone encroached into the reservoir more and more for base pressures greater than about 110 bar. Thus to achieve a fairly uniform vapour saturation in the reservoir and to

achieve deep reservoir pressure and temperature of 39.1 bar and 249°C (typical of Darajat) a base pressure of 94.6 bar was used. Figure 3 shows the vapour saturation distribution for Model 1b.

As the irreducible water saturation is high the vapour saturation is low, even in the reservoir.

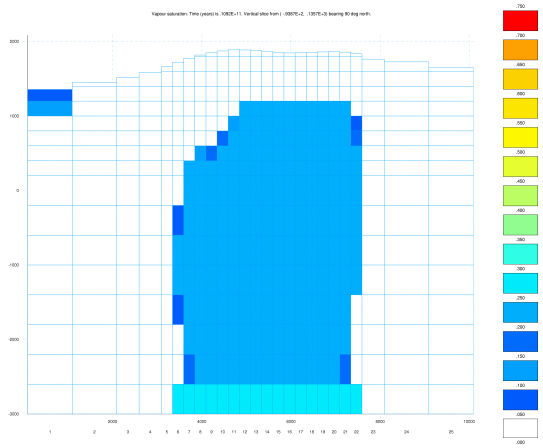

Figure 3: Vapour saturation distribution for Model 1b.

Table 3: Catalogue of models.

Model 1a- parameters given in Table 1 and 2.
Model 1b- Model 1a + simpler permeability distribution +low spring COP and low base pressure
Model 2- deliverability parameters
a) Model 1b + high COP (20 bar) + high MSF(20 kg/s)
b) Model 1b + high COP (20 bar) + low MSF(5 kg/s)
c) Model 1b + low COP (15 bar) + high MSF(20 kg/s)
d) Model 1b + low COP (15 bar) + low MSF(5 kg/s)
Model 3- relative permeability curves;
a) Model 2 (d) + Linear#2
b) Model 2 (d) + Grant
Model 4- Model 3 (b) + low vertical permeability
Model 5- Model 3 (b) + low porosity
Model 6- Model 3 (b) + different reinjection rates
a) No-injection b) 15% c) 35% d) 50% e) 75%
Model 7- Model 6 (b) + late start of reinjection
Model 8- refined grid + parameters of Model 6 (b)
a) one-grid scheme
b) two-diagonal grid scheme
Model 9- Model 6 (b) + embedded radial grid
Model 10- Model 8 (a) + embedded radial grid
Model 11- Model 6 (b) + fractured grid
a) 5% fracture volume
b) 6% fracture volume
Model 12- Very fine grid with the parameters of Model 6 (b)
Model 13- Model 12 with 9-point differentiation

COP: Cut-off pressure MFS: Maximum steam flow

2.2 Production and Injection

In the next stage of modeling, production and injection strategies were investigated. In the 3D Darajat model production is taken from levels equivalent to layers EE and GG, and therefore production blocks were assigned to these layers in the 2D model. Three production wells, each producing from two layers, were allocated (as shown in Figure 1 with red squares). The injection wells were located above the production wells (blue squares in Figure 1). The production and injection parameters for Model 2a are shown in Table 4 For the injection wells the PINJ option (autough2 notes, (2002)) was used which allows a fraction of the production from a group of wells to be injected into another well.

Table 4: Production and injection parameters, Model 2a

production	**injection**
Deliverability option: DELG	Deliverability option: PINJ
Productivity index: 1.09E-9 m^3	Injectivity index: 1.09E-9 m^3
Cut-off pressure: 20 bar	Injection enthalpy: 125.7 kJ/kg
Maximum steam flow: 20 kg/s	Injection fraction: 25% of steam production

Figure 4 shows the steam production rate for this model, for two cases: injection (blue) and no-injection (red). According to this figure there is no significant difference in steam production between the injection and no-injection cases.

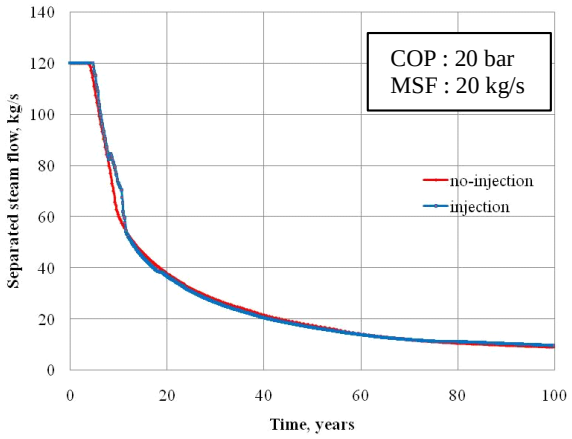

Figure 4: Steam production rates for injection (blue) and no-injection (red) for Model 2a

3. MODIFICATIONS TO THE MODEL

Unfortunately the results shown in Figure 4 are counter to past experience. Field experiences from vapour dominated systems like Larderello and The Geysers shows that infield reinjection has an important role in maintaining steam production (Cappetti, G., et al., 1995, Sanyal, 2000). Therefore it was decided to investigate various modifications to Model 2.

3.1 Deliverability of Production Wells

In Model 2 the production wells operate on deliverability against a prescribed cut-off pressure, with a set productivity index PI and maximum steam flow. In this section we investigate the effect of each deliverability parameter individually to determine their impact on steam production.

First for Model 2b the maximum steam flow was decreased from 20 kg/s to 5 kg/s for each well. The results in Figure 5(a) show that during the first 70 years of production, injection does not have any effect on steam flow, but after that it produces a small increase in steam production.

Secondly in Model 2c, the cut-off pressure was decreased from 20 bar (high cut-off pressure) to 15 bar (low cut-off pressure). The cases of 20 kg/s maximum steam flow and 5 kg/s maximum steam flow (Model 2d) were both run. Results are shown in Figure 5(b) and 5(c), respectively. Figure 5(c) shows that for the case including both a lower maximum steam flow and a lower cut-off pressure, injection has a considerable positive effect on steam production. Whereas with only a lower cut-off pressure (Figure 5(b)) or only a lower maximum steam flow (Figure 5(a)) injection has little effect.

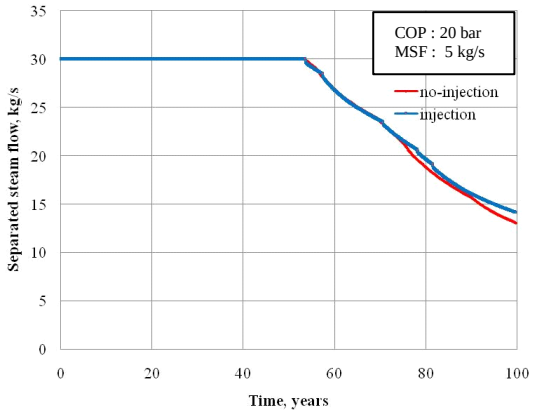

(a)

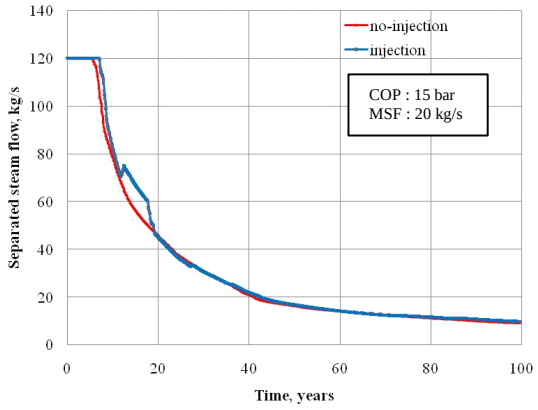

(b)

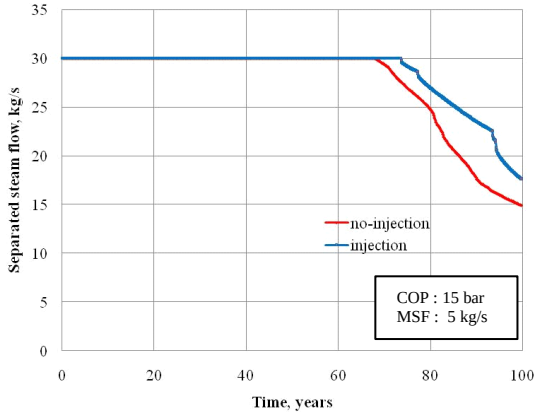

(c)

Figure 5: Steam production rates (a) low maximum steam flow, high cut off pressure (Model 2b), (b) low cut-off pressure, high maximum steam flow (Model 2c), (c) low cut-off pressure and low maximum steam flow (Model 2d). Injection (blue) and no-injection (red).

Since the difference between the injection and no-injection cases is highest for Model 2d, with a low cut-off pressure and low maximum steam flow, it was used for the further modifications discussed in the rest of this section.

3.2 Relative Permeability

Bodvarsson et al. (1980) showed that the choice of steam-water relative permeabilities has a significant impact on the performance of models of geothermal reservoirs. In this section our particular interest is to vary the immobile liquid and vapour saturation values and the shape of the relative permeability curves to find the best options for modeling vapour dominated systems.

Table 5 shows the different relative permeability cases which were tried at this stage of the study. Linear#1 is the relative permeability function used in the 3D Darajat model and for Models 1 and 2 above. A second linear relative permeability function was tried (Model 3a) with a smaller residual liquid saturation (called Linear#2 here). As expected the lower residual liquid saturation results in higher vapour saturations in the model (see Figure 6).

Table 5: Relative permeabilities.

Relative permeabilities	immobile liquid saturation	immobile vapour saturation	perfectly mobile liquid saturation	perfectly mobile vapour saturation
Linear # 1	0.75	0.0	1.0	0.25
Linear # 2	0.25	0.0	1.0	0.75
Grant's Curve	0.1	0.0		

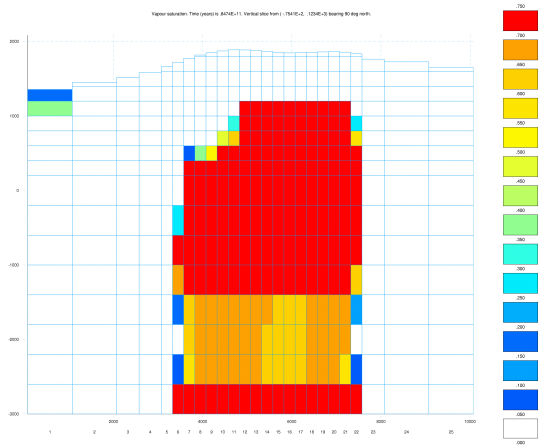

Figure 6: Natural state vapour saturation distribution for Linear#2 relative permeabilities.

Some adjustments of the model parameters were required to obtain similar pressure and temperature profiles with Model 2d and Model 3a. The cut-off pressure for the spring blocks in the Linear#2 model was increased from 20 bar to 22.5 bar. The comparison of the natural state temperature and pressure profiles for the models using Linear #1 with Linear#2 is shown in Figure 7. For the model using Linear#1, the total mass flow from spring blocks is 3.25 kg/s while it is 2.85 kg/s for Linear#2.

Figure 8 shows the steam production rates for Model 3a for the cases of injection and no-injection. According to this figure, the higher vapour saturations in the reservoir with

the use of the Linear#2 relative permeability causes the steam flow to drop much earlier (compare with Figure 5(c)). Again injection increases the steam production.

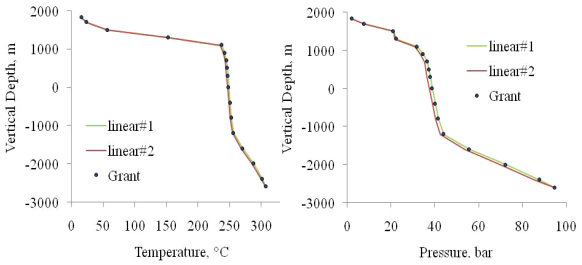

Figure 7: Comparison of temperature and pressure profiles of 2D models using Linear#1, Linear #2 and Grant's curves relative permeabilities.

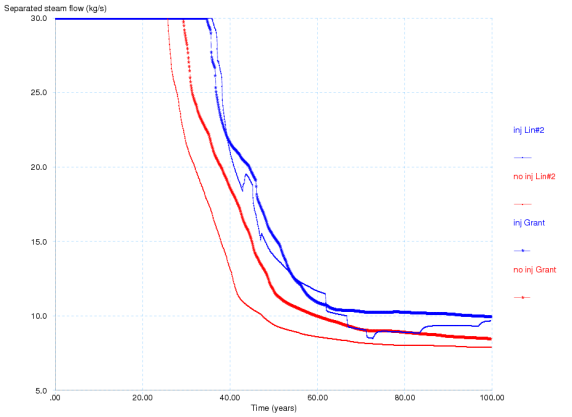

Figure 8: Steam production rates for injection (blue) and no-injection (red) using Linear#2 and Grant's curves for relative permeabilities.

However as shown in Figure 8, in the injection case some sudden increases and decreases in the steam flow occur. In a study of a 1-D vertical approximation of Larderello, Schroeder et al (1982) found similar oscillations. They found out that amplitude and frequency of the oscillations depends on the space discretization, on the difference between initial temperature and saturation temperatures in the elements penetrated by the liquid water and on the shape of the relative permeability curves. Bodvarsson et al. (1985) experimented with different relative permeability curves to analyse mobility effects. They pointed out that the Corey curves may not be suitable for modelling fractured geothermal reservoirs since the predicted steam production rate strongly depends on the assumed initial vapour saturation.

Therefore at this stage of study it was decided to use Grant's curves applied to Model 2d. This new model was named Model 3b. As shown in Figure 7, it was possible with Model 3b (black symbol) to obtain a good match to the natural state pressure and temperature profiles for Model 2d (red line) which uses the Linear#1 relative permeability curves.

Figure 8 shows that using Grant's curve increases the amount of steam production. This result is to be expected since Grant's curve gives a higher gas relative permeability. Figure 8 shows that using Grant's curve decreases the amplitude of the oscillations and smoothes the sharp changes in the steam flow. Therefore Grant's curves were used for the models investigated in the rest of the study.

3.3 Vertical Permeability

The performance of a vapour-dominated reservoir under production depends on how quickly it runs out of liquid water and becomes superheated. One of the factors that affect this process is the recharge of the reservoir zone by steam and water flowing upwards through the reservoir. This effect is in turn controlled by the vertical permeability. In this section anisotropic reservoir permeability is introduced to determine the effect of changes in vertical permeability on steam production.

Using Model 3b, the vertical permeability of four rock types (brccm, brcch, ande, andd) representing the reservoir blocks was decreased by a factor of two and the new model was named Model 4.

This modification increased the temperatures and pressures in the natural state of the system (see Figure 9). It resulted in a slight increase in the steam flow for the injection case at an earlier time. However after about 50 years the lower vertical permeability case starts to produce less steam than the case using isotropic permeability in the reservoir (see Figure 10). Since decreasing the vertical permeability altered the natural state significantly and does not modify the effect of injection on steam flow, this case was not considered further.

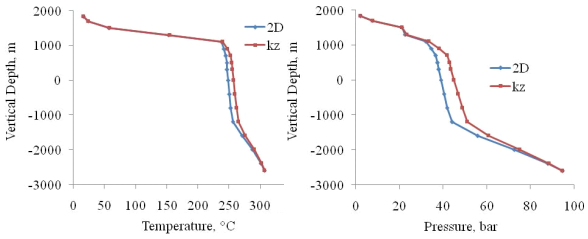

Figure 9: Comparison of temperature and pressure profiles of Model 3b with profiles from Model 4 (decreased vertical permeability).

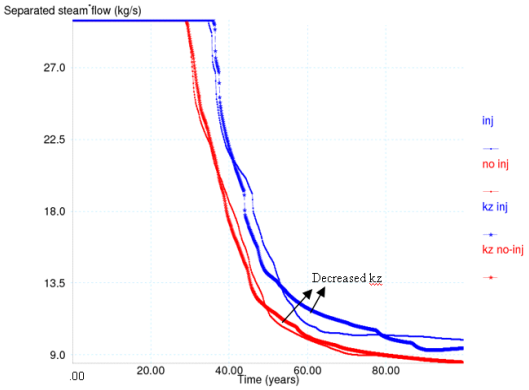

Figure 10: Steam production rates for injection (blue) and no-injection (red), with and without a vertical permeability decrease.

3.4 Porosity

In this section the case of lower reservoir porosity was tried to investigate whether or not a change in porosity has a significant impact on the effect of injection. Starting with Model 3b, the porosity in two rock types, brccm and brcch, was decreased from 0.09 to 0.07 and for rock types andd and ande it was decreased from 0.06 to 0.04. This new model was named Model 5.

Figure 11 shows the expected effect that decreasing porosity reduces the available water and steam and therefore reduces the steam flow. However decreasing the porosity of the reservoir rocks does not change the effect of injection on steam flow. In both cases the extra steam flow resulting from injection is similar in magnitude. Therefore the porosity of the reservoir rock was not changed for the further cases considered below.

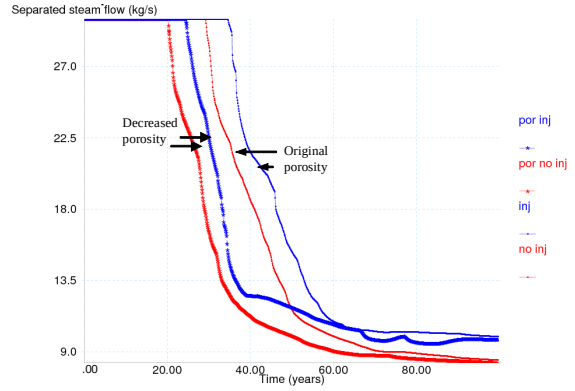

Figure 11: Steam production rates for injection (blue) and no-injection (red) for decreased reservoir porosity and the original reservoir porosity.

3.5 Injection Rates

Since the amount of injected fluid is an important parameter to consider while deciding on the injection strategy, in this section different injection rates were tried. Until this stage, as shown in Table 4, for all cases an injection rate equal to 25% of the produced steam was applied. To see the effect of varying the injection rate on steam flow, four more injection rates were tried, namely, 15, 35, 50, 75% of the total produced steam. These models were named Model 6a, 6b, 6c and 6d, respectively.

Results shown in Figure 12 indicate that, for the 15, 25, 35, 50% cases, increasing the injection rate extends the lifetime of the reservoir. The results are variable but overall up to the 50% injection rate an increase in injection rate causes an increase in steam production. But for the case of a very high injection rate (75%) the duration of production at the maximum steam flow is a small amount shorter than for the 50% case.

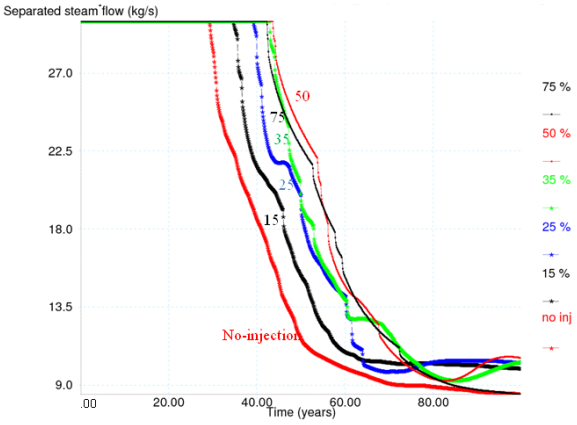

Figure 12: Steam production rates for different injection rates

The reason for the decline of steam flow in this case is proximity of the production and injection wells. The enthalpy of steam from the production wells that are near the injection wells declines as a result of breakthrough of the injected water. Therefore Figure 12 shows that in general cold water injection into vapour dominated zones enhance the productivity of steam wells. However for the case of a very high injection rate beneficial effect of injection is lessened.

3.6 Start Time for Injection

Review of previous injection experiences indicates that for some geothermal fields injection commenced after several years of exploitation. This occurred in some cases as a result of environmental problems and the introduction of new regulations, and in other cases in order to prevent further pressure decline and subsidence caused by the production (Kaya et al. (2007)). In this section to investigate the effect of different start times for injection on steam production, we introduce a new model with injection starting after 20 years of production, (Model 7).

Figure 13 indicates that if injection starts late, the beneficial effect of injection also occurs later. Thus an early start for injection is the best strategy.

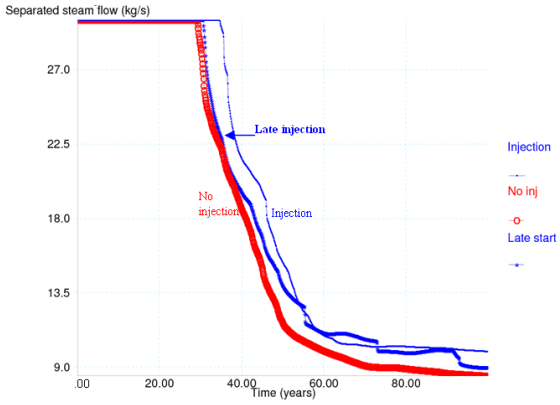

Figure 13: Steam production rates for no-injection, injection starting after 0 years and after 20 years of production.

3.7 Grid Refinement

Space discretization effects are well known in modeling immiscible displacement processes (Aziz and Settari, 1979). These effects also arise in modeling two-phase flow with phase changes, because it involves coupling between fluid flow and heat transfer and a varying saturation of the flowing two-phase mixture (Pruess, 1991). The discretization of space and time introduces truncation errors, which generally become smaller when the mesh is refined. Schroeder et al. (1982) showed that the amplitude and frequency of spurious oscillations in the solution depend on the level of space discretization, and they concluded that a finer mesh will reduce the amplitude and increase the frequency of the oscillations.

To investigate the effects of space discretization on steam production, we refined the grid blocks in the production region horizontally and vertically, dividing each grid block into four. This new model was named Model 8.

Refining the grid blocks and using the same basement boundary conditions, the same heat inputs and the same deliverability parameters as for the coarse model (Model 6b) caused a slight increase in the natural state pressure and temperature profiles for the fine model (Model 8). To

improve the match to the natural state conditions the cut-off pressure for the spring blocks in the fine model was decreased from 20 bar to 18 bar.

For assigning a well in one block in the coarse model to four blocks in the fine model two different schemes were investigated:

1- One block: left lower (Model 8a),

2- Two diagonal blocks: left lower and right upper (Model 8b).

Trials showed that using the two diagonal blocks gives closer results to the coarse grid model.

As shown in Figure 14, Model 8b with the refined grid predicts a slightly faster drop in steam flow.

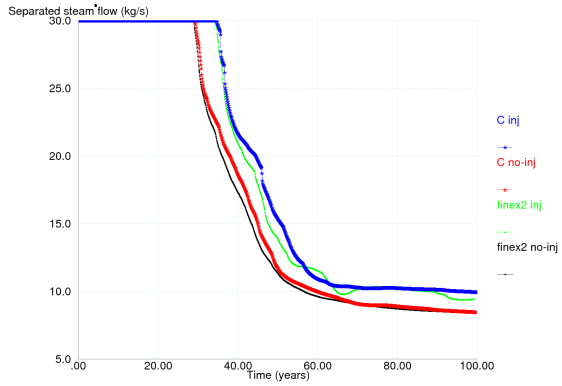

Figure 14: Comparison of steam production rates for Model 6b (coarse grid) and Model 8b (fine model) for injection and no-injection.

3.8 Embedded Radial Grid Near the Wells

Near the well there is low pressure and high vapour saturation which is not possible to represent accurately by a large block. For more accurate representation of near-well behaviour, it was decided to embed a radial grid within the blocks that contain wells. Embedded radial grids were used with both the coarse model and the fine model.

1- Model 9, coarse model with an embedded radial grid; A radial sub-grid of 26 blocks was embedded in each production block. The grid structure of the production block is shown in Figure 15. The volume of the radially refined section (shown in yellow in Figure 15) is half of the total block volume. The radial block thickness increases with a 1.20 expansion factor.

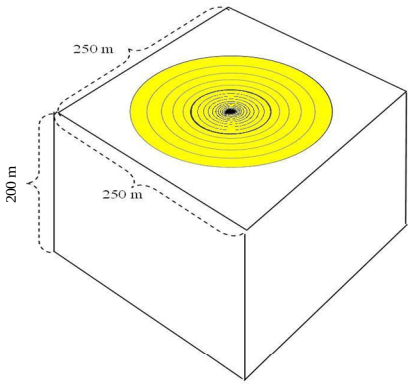

Figure 15 Grid structure of the coarse model with an embedded radial grid.

Figure 16 compares the coarse model results (Model 6b) with the same model with an embedded radial grid (Model 9). This figure shows that the results from Model 9 with the radial grid embedded are significantly different to those from the standard coarse model. For Model 9 the steam productions start to decrease earlier than for Model 6b. However the steam production decreases more quickly in the coarse model.

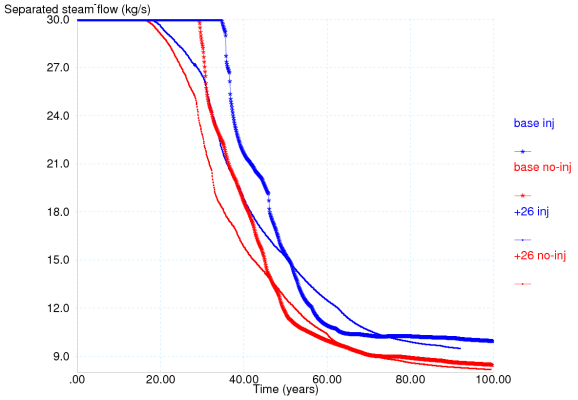

Figure 16: Comparisons of steam production rates for the coarse model with and without a radial grid embedded.

2- Model 10, fine model with embedded radial grids; Similarly a 21 radial sub-grid was placed into the production blocks of the fine model (Model 8a). The grid structure of the production block is shown in Figure 17. The sub-grid used here is the same as the first 21 blocks of the sub-grid used in Model 9. The total volume of the radial grid (shown in blue in Figure 17) is 31% of the total block volume of the fine grid.

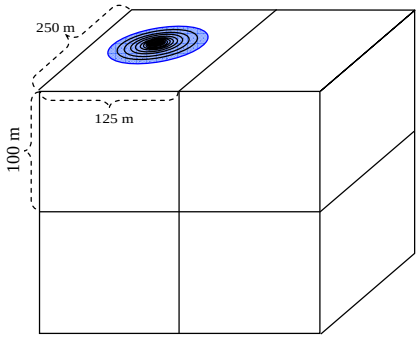

Figure 17: Grid structure of the fine model with an embedded radial grid.

Figure 18 compares steam production rates for Model 8a (fine model) with those for Model 10 (fine model with an embedded radial grid). According to this figure, as for the coarse model results shown in Figure 16, the steam productions start to decrease much earlier in Model 10 than for Model 8a.

Additionally it can be observed from Figure 16 and Figure 18 that using the embedded radial grid eliminates the oscillations in steam production for the injection case.

3.9 Fractured Rock Model

In a vapour-dominated system steam moves through fractures and heat from the surrounding rock matrix causes the immobile water in the fractures to boil, thus creating more steam. In the models discussed above the fractured

rock is represented as a porous medium but in this section we consider a double porosity approach treating the fractures more explicitly (see Warren and Root, 1963 and Barenblatt et al., 1960).

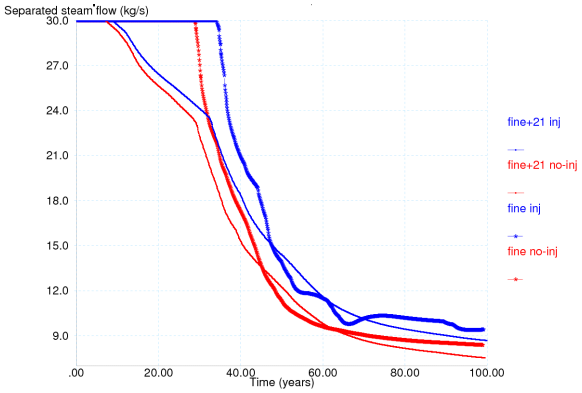

Figure 18: Comparisons of steam production rates of the fine model with and without an embedded radial grid.

Pruess and Narasimhan (1985) introduced the multiple-interacting continua (MINC) method, as a generalization of the dual-porosity concept. The main transport of fluids takes place through the fractures, while the matrix blocks supply heat and some fluid to the fractures. In this method, each reservoir block is divided into a nested arrangement with a matrix sub-domain adjacent to a fracture sub-domain. Pruess and Narasimhan implemented this formulation in the Integral Finite Difference (IFD) framework used in TOUGH2.

In this study Model 6b used as the base model and a MINC model is set up with the parameters shown in Table 6. The new model was named Model 11a.

Table 6: Parameters used in the fractured rock model

Total number of MINC	3
Type of proximity function	TWO-D
Matrix block thickness	5.0 m
Volume fraction of the fracture continuum	5%
Volume fraction of the matrix continuum	50%, 45%
Matrix porosity	0.01
Fracture porosity	0.9

A proximity function for calculating the MINC grid volumes and connection areas was chosen based on two sets of plane parallel infinite fractures (TWO-D), with arbitrary angle between them. A schematic of the fracture and two matrix continua are shown in Figure 19. The MINC partitioning was applied to eight layers of the reservoir (andd, ande, brcch and brccm rock types) and produced 108×3=324 blocks. The fracture permeability was put equal to the corresponding permeability in the porous medium model (Model 6b). A matrix permeability 1/10 of the fracture permeability was assigned.

Figure 20 compares steam production rates for the porous medium model and the fractured medium model. For the fractured medium model, steam production drops earlier than for the porous medium model, for both the injection and no-injection cases. This is to be expected as the MINC model has a lower average porosity (5.45%), and as was seen in Section 3.4, a lower porosity reduces the available fluid and decreases the steam flow. In the long term, after 70 years of production there is no apparent difference on steam production between the porous and fractured medium models.

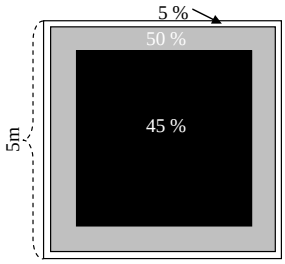

Figure 19: MINC - discretization for the fractured rock model (Model 11a).

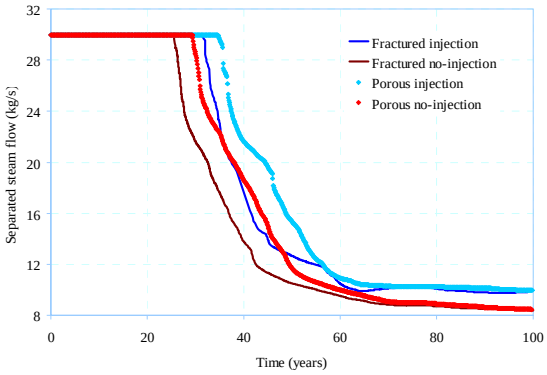

Figure 20: Steam production rates for a porous medium (Model 6b) and fractured medium (Model 11a) models. Injection and no-injection.

To assign approximately the same pore volume in both the porous medium and fractured medium models, a new model was set up (Model 11b) with the volume fraction for the fractures increased to 6% and matrix continuum volumes set to 50% and 44%. In this case the average reservoir porosity of the fractured medium model is 6.3%. This value is similar to the average for the porous medium model as most of the reservoir has a porosity of 6% while the remainder has a porosity of 9%. Comparisons of the results are shown in Figure 21. This figure shows that there is no significant difference in the steam production from the porous medium and fractured medium models. Therefore when the pore volumes of the two types of model were consistent, introducing double porosity into the model did not change the rate of steam production or the effect of injection significantly.

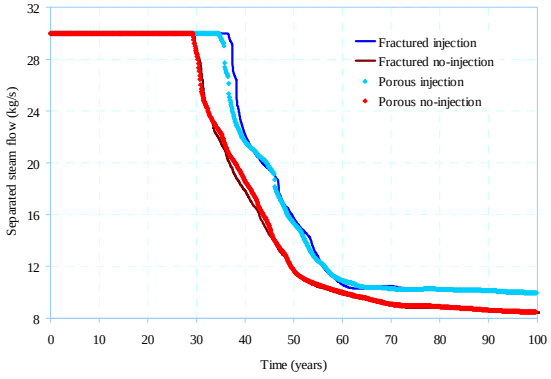

Figure 21: Steam production rates for a porous medium (Model 6b) and fractured medium (Model 11b) models. Injection and no-injection.

3.10 Nine-Point Differencing

In the literature strong grid orientation errors have been observed in areal 2-D simulations of steam flooding of petroleum reservoirs. Todd et al., (1972) compared a diagonal grid and a parallel grid in a five-spot grid, and demonstrated that the predicted recovery performance depends on the grid orientation and the diagonal grid gave more accurate results in water-flood calculations up to adverse mobility ratio of 10. Coats et al., (1974) simulated steam injection into an oil reservoir and found that grid orientation has a great effect on an unfavourable mobility-ratio displacement. Brand et al., (1991) demonstrated that the grid orientation effect is a result of coupling between the anisotropic numerical diffusion and the physical instability of the displacement front.

Yanosik and McCracken (1979), Coats and Ramesh (1982), and Pruess and Bodvarsson (1983) showed that grid orientation effects can be substantially reduced by means of a "nine-point" approximation, which allows for the possibility of flow along diagonal directions. Pruess (1991) and Pruess (1995) demonstrated that grid orientation effects are aggravated when vertical flow is taken into consideration. These studies indicate that, grid orientation effects can be much reduced by using 9-point differencing method.

3.10.1 Nine-Point, Finite-Difference Formulation

The standard five-point formulation considers only the flows between the centre block and the four nearest-neighbour blocks that are adjacent to its sides, top and base. (in Figure 22 block O communicates with blocks E, N, W and S).

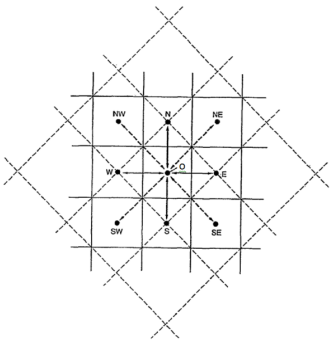

Figure 22: Five and nine-point finite difference approximations.

The nine-point formulation considers this flow as well as the flow between the block and the four blocks located at its corners (block O also communicates with blocks NE, NW, SW and SE).

The basic mass and energy balance equations can be written in discrete form as follows:

$$V_i \frac{A_i^{n+1} - A_i^n}{\Delta t} = \sum_j a_{ij} F_{ij}^{n+1} + q_i^{n+1} \qquad (3)$$

Where A_i^n is the mass or energy per unit volume in block i at time $n\Delta t$, F_{ij}^n is the mass or energy flux from block i to block j, and q_i^n is the flow to sinks or sources (that is, production or injection wells). The volume of block i is V_i and the area connecting block i to block j is a_{ij}.

The general expression for 9-point flux terms is (Forsythe and Wasow, (1960); Pruess and Bodvarsson, (1983)

$$\left(\sum_{\bar{m}} A_{nm} F_{nm}\right)_{9-point} = \frac{2}{3}\left(\sum_{\bar{m}} A_{nm} F_{nm}\right)_{parallel} + \frac{1}{3}\left(\sum_{\bar{m}} A_{nm} F_{nm}\right)_{diagonal} \qquad (5)$$

Where the notation "parallel" indicates flux terms arising from the standard 5-point difference approximation while "diagonal" indicates flux terms across grid block corners.

Therefore the implementation of the nine-point approximation requires following steps,

(i.) An input file was created containing geometric parameters grid volumes, interface areas and distances between gridblocks appropriate for the conventional five-point method.

(ii.) All interface area in the "parallel" grid were reduced by a factor 2/3

(iii.) A list of "diagonal connections (containing interface areas and distances between gridblocks) were appended.

3.10.2 Model for Nine-Point Approximation

The implementation of nine-point differencing used here requires a laterally regular grid with square grid blocks. Thus a very fine model (Model 12) with a uniform horizontal and vertical spacing of 100 m was created.

The parameters from Model 8b were used with this new grid structure. By changing the boundary pressure of the bottom of the reservoir from 94.6 to 96.6 bar and by setting the cut-off pressure for the spring wells to 27.5 bar a good match of the natural state conditions from the coarse and very fine models was obtained. Spring and production blocks were located into two-diagonally opposite grid-blocks (left lower and right upper) of the refined grids.

3.10.3 Implementation of Nine-Point Differencing

Nine-point differencing was implemented in only the reservoir layers (Model 13). Figure 23 (a) and (b) shows vapour saturation distribution for five-point and nine-point differencing methods respectively, after 100 years of production. From these figures it can be observed that for the five-point method injected water flows downward, forming a tall thin plume.

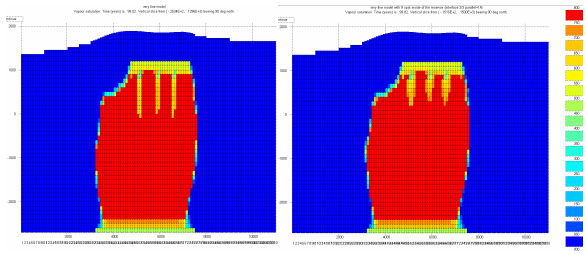

(a) (b)

Figure 23: Vapor saturation distributions after 100 years of production and injection case a) five-point b) nine-point

Introducing the possibility of diagonal flow with the nine-point approximation allows the representation of the lateral movement of the wetter injection plume and creates a larger central section of the plume. Therefore the wetter zone

around the production wells better supports the pressure of reservoir and allows the production of more steam.

Figure 24 shows the comparisons of steam flows for models using five-point and nine-point approximations. Although this figure does not show much difference between using the 5-point or the 9-point approximation for the injection case, it does show the elimination of spurious oscillations by the use of high order differencing.

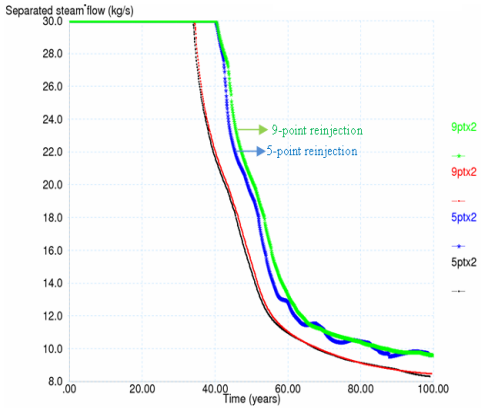

Figure 24: Comparisons of steam flows for models using five-point and nine-point approximations.

4. SUMMARY AND CONCLUSIONS

The goal of this paper was to provide a good model which produces accurate and realistic predictions of injection effects on vapour-dominated two-phase reservoirs. In particular we tried to obtain a model which exhibits behaviour representative of vapour dominated reservoirs such as Larderello or The Geysers where infield injection has an important role in maintaining steam production.

These investigations can be summarized as follows:

Base conditions: Modelling experiments showed that increasing the base boundary pressure increased the reservoir pressure up to a certain value, then it decreased. Thus a particular reservoir pressure can be obtained with two base boundary conditions. However it was found that the higher base pressure resulted in a wetter reservoir and therefore the lower boundary pressure was preferred.

Deliverability of production wells: Our investigation showed that a lower cut-off pressure in the deliverability formula resulted in a larger effect of injection on the steam flow.

Relative permeability: Three different relative permeability formulae were tried. Using a low value of irreducible liquid saturation and high perfectly mobile vapour saturation increased the vapour saturation in the reservoir and decreased the steam flow. The use of Grant's curves decreased the oscillations in the production/injection simulations.

Porosity and vertical permeability: Changes in porosity and vertical permeability were tried in the model to see if changes in these parameters affect steam production if injection is included. The simulation results showed no significant effect, with the relative effect of injection being very weakly affected by changes in these parameters.

Reinjection rates and start time for reinjection: Trials showed that starting injection at the same time as production gives the best steam output.

Fractured rock model: When the pore volume of the porous and fracture models was consistent, introducing a double porosity model to the system, based on a MINC partitioning process did not effect steam production significantly. Also effect of injection did not depend on whether a porous medium model or a fractured medium model was used.

Grid size and orientation: To analyse the sensitivity of the model results to grid size and orientation, mesh refinement and radial embedded grids near production wells were tried. Our investigations showed that using a finer grid gives only slightly different results. The steam flow starts to drop from its maximum value sooner but over the long term there is little difference between the coarse grid and fine grid results. However applying an embedded radial grids near the wells produce different results for the steam flow.

Nine point approximation: Representation of the movement of injection plume through diagonal grids as well as parallel grids did not effect steam production significantly but using high order differencing eliminated the spurious oscillations which occur in the injection case.

REFERENCES

autough2 notes, 2002. Notes for using autough2 (the Auckland University version of TOUGH2). Last modified 17 October 2002.

Alamsyah, O., Bratakusuma, B., Hoang,V. and Roberts, J.W., 2005. Dynamic modeling of Darajat Field using numerical simulation. Proceedings of World Geothermal Congress 2005, Antalya, Turkey, 24-29 April 2005.

Aziz, K. and Settari, A., 1979. Petroleum Reservoir Simulation. Elsevier, London.

Barenblatt, G. I., Zheltov, Yu. P., and Kochina, I. N., 1960. Basic concepts in the theory of seepage of homogeneous liquids in fissured rocks. Prikl. Mat. i Mekh., Soviet Appl. Math. Mech., 24(5), pp. 852–64.

Bodvarsson, G.S., O'Sullivan, M.J., and Tsang, C.F., 1980. The sensitivity of geothermal reservoir behavior to relative permeability parameters. Proceedings of Sixth Workshop on Geothermal Reservoir Engineering, Stanford, CA, Dec. 16-18, 1980.

Bodvarsson, G.S., Pruess, K., O'Sullivan, M.J., 1985. Injection and energy recovery in fractured geothermal reservoirs. Soc. Pet. Eng. J., 25(2), pp. 303-313.

Brand, C. W., Heinemann, J. E. and Aziz, K., 1991. The grid orientation effect in reservoir simulation. Paper SPE-21228, presented at the Society of Petroleum Engineers Eleventh Symposium on Reservoir Simulation, Anaheim, CA, U.S.A.

Cappetti, G. and Ceppatelli L., 2005. Geothermal Power Generation in Italy, 2000–2004 Update Report. Proceedings of the World Geothermal Congress, Antalya, Turkey, 24-29 April, 2005

Cappetti, G., Parisi,L., Ridolfi, A. and Stefani, G., 1995. Fifteen years of reinjection in the Larderello-Valle Secolo area: analysis of the production data. Proceedings of the World Geothermal Congress, 18-31 May. 1995. Florence, Italy.

Coats, K. H., George, W. D., Chu, C. and Marcum, B. E., 1974. Three-dimensional simulation of steam-flooding. Soc. Pet. Eng. J., pp. 573-592.

Coats, K. H. and Ramesh, A. B., 1982. Effects of grid type and difference scheme on pattern steamflood simulation results. Paper SPE-11079, presented at the 57th Annual Fall Technical Conference and Exhibition of the Society of Petroleum Engineers, New Orleans, LA, U.S.A.

Forsythe, G. E. and Wasow, W. R., 1960. Finite-difference methods for partial differential equations. John Wiley. New York.

Goyal, K. P., 1998. Injection related cooling in the Unit 13 area of the Southeast Geysers. Proceedings of Twenty-Third Workshop on Geothermal Reservoir Engineering, Stanford University. Stanford, California, January 26-28. 1998. pp. 397-405.

Hadi, J., Harrison ,C., Keller, J., Rejeki, S., 2005. Overview of Darajat reservoir characterization: a volcanic hosted reservoir. Proceedings of the World Geothermal Congress 2005, Antalya, Turkey, 24-29 April 2005.

Kaya, E., Zarrouk, S. and O'Sullivan, M. J., 2007. Reinjection in geothermal fields: a worldwide review and analysis. Technical Report, No. 657, Department of Engineering Science, The University of Auckland, New Zealand.

McGuinness, M. J., Blakeley M., Pruess, K. and O'Sullivan, M. J., 1993. Geothermal heat pipe stability: solution selection by upstreaming and boundary conditions. Transport in Porous Media 11, pp. 71-100.

O'Sullivan, M.J., 1990. A simple model of a vapour-dominated geothermal reservoir. Proceedings of the TOUGH Workshop, Lawrence Berkeley Laboratory Berkeley, California, September 13-14, 1990, pp. 37-43.

O'Sullivan, M.J., Pruess, K., Lippmann, M.J., 2001. State of the art of geothermal reservoir simulation. Geothermics 30 (4), pp. 395-429.

Pruess, K. and Bodvarsson, G. S., 1983. A seven-point finite difference method for improved grid orientation performance in pattern steam floods. Paper SPE-12252, presented at the Seventh Society of Petroleum Engineers Symposium on Reservoir Simulation, San Francisco, CA, U.S.A.

Pruess, K., Narasimhan, T.N., 1985. A practical method for modeling fluid and heat flow in fractured porous media. Soc. Pet. Eng. J., 25 (1), pp. 14–26.

Pruess, K., Calore, C., Celati. R. and Wu, Y. S., 1987. An analytical solution for heat transfer at a boiling front moving through a porous medium. Int. J. of Heat and Mass Transfer, 30, (12) pp. 2595-2602.

Pruess, K., 1991. Grid orientation effects in the simulation of cold water injection into depleted vapor zones. Proceedings of Sixteenth Workshop on Geothermal Reservoir Engineering, Stanford University, Stanford, California, January 23-25, 1991, SGP-TR-134, pp.211-220.

Pruess, K., 1992. Brief guide to the MINC-method for modeling flow and transport in fractured media. Report LBL-32195, Lawrence Berkeley Laboratory Berkeley, CA, May 1992

Pruess, K., 1994. Liquid phase dispersion during injection into vapor-dominated reservoirs. Proceeding of Ninth Workshop on Geothermal Reservoir Engineering 1994, Stanford University, Stanford, California, January 18-20, 1994, pp. 43-49.

Pruess, K., 1995. Numerical simulation of water injection into vapor-dominated reservoirs. Proceeding of the World Geothermal Congress 1995, Florence, Italy, May 1995, pp. 1673-79.

Pruess, K., 1996. Injection plume behaviour in fractured, vapor-dominated reservoirs. Proceeding of Twenty-First Workshop on Geothermal Reservoir Engineering, Stanford University, Stanford, California, January 22-24, 1996, SGP-TR-151. pp. 413-420.

Pruess, K., Oldenburg, C., Moridis, G., 1999. TOUGH2 User's Guide, Version 2.0. Lawrence Berkeley National Laboratory, Earth Sciences Division, Berkeley, California.

Pruess, K. and Garcia, L., 2000. A systematic approach to local grid refinement in geothermal reservoir simulation. Proceedings of the World Geothermal Congress 2000, Kyushu - Tohoku, Japan.

Sanyal, S.K., 2000. Forty years of production history at The Geysers geothermal field, California - The lessons learned. Geothermal Resources Council Transactions, 2000. **24** (September 24-27): pp. 317-323.

Schroeder, R. C., O'Sullivan, M. J., Pruess, K., Celati, R. and Ruffilli, C., 1982. Reinjection studies of vapor-dominated systems. Geothermics, 11(2), pp. 93-119

Todd, M. R., O'Dell, P. M. and Hirasaki, G. J., 1972. Methods for increased accuracy in numerical reservoir simulators. Soc. Pet. Eng. J., pp. 515-530.

Warren, J.E. and Root, P.J., 1963. The behavior of naturally fractured reservoirs, Soc. Pet. Eng. J., Transactions, AIME, 228(3), pp. 245-255

Yanosik, J.L. and McCracken, T.A., 1979. A nine-point, finite difference reservoir simulator for realistic prediction of adverse mobility ratio displacements. Soc. Pet. Eng. J., 19(4), pp. 253-262.